

# Enhancement of Seebeck coefficient with full spin polarization of CsMgN<sub>2</sub> thin films: a DFT study

Rohangiz Ashtari Faregh<sup>1</sup>, Arash Boochani<sup>2,3\*</sup>, Seyedeh Razyeh Masharian<sup>1</sup>

<sup>1</sup>Department of Physics, Hamedan Branch, Islamic Azad University, Hamedan, Iran.

<sup>2</sup>Department of Physics, Kermanshah Branch, Islamic Azad University, Kermanshah, Iran.

<sup>3</sup>Quantum Technologies Research Center (QTRC), Science and Research Branch, Islamic Azad University, Tehran, Iran.

\*Corresponding author: arash-bch@yahoo.com

Received 25 January 2023; Accepted 23 February 2023; Published online 27 February 2023

## Abstract:

Structural, electronic, and thermoelectric properties of the CsMgN<sub>2</sub> compound with its thin film films of Cs-Mg and Mg-N terminations have been studied in a First-Principles study. The total energy changes (E-V) versus the unit cell volume of bulk show better stability in the ferromagnetic than the non-magnetic phase. The E-V diagrams of film Cs-Mg and Mg-N terminations have the ground state points at the ferromagnetic phase. The derivative bulk modulus of Cs-Mg termination is like the bulk phase, which refers to the ionic bonds between atoms.

The magnetic moment of the bulk and two mentioned terminations have the integers of 3  $\mu_B$ , 10  $\mu_B$ , and 13  $\mu_B$ , respectively. The DOS and bandstructure diagrams by the mBJ and GGA approximations confirm the half-metallic behavior of the bulk and the mentioned terminations. The energy gaps of their semiconductor phase are 1.40 eV, 0.64 eV, and 0.20 eV, for the bulk, Cs-Mg, and Mg-N terminations, respectively. The Seebeck coefficient of Cs-Mg termination in 200 K temperature is much higher than the bulk case. The merit figure of coefficient (ZT) shows that bulk and mentioned terminations have high thermoelectric quality at up spin.

**Keywords:** DFT; Seebeck coefficient; CsMgN<sub>2</sub>; Electronic; Thermoelectric

## 1. Introduction

After de Groot's discovery in 1983 [1], studies on the half-metals have emerged in solid-state physics. Many studies were started to understand, predict and develop new half-metal materials. The main focus of the research was on half-metallic materials that could be used in the spintronics industry as magnetic random access memory (MRAM) [2–4]. Many spintronic features, such as the shape memory effect [5, 6], the giant magneto-thermal effect [7–9], and the giant magneto-resistance effect [10, 11], were found in Heusler compounds.

The transition metal elements are present in most Heusler compounds, and because of their half-filled d orbitals, they often play an essential role in half-metallic behavior. Recently, a new class of half-Heusler compounds with 100% spin polarization has been discovered. Their crystal structure does not contain transition metal atoms, called sp or d<sub>0</sub> half-metallic materials. So far, these d<sub>0</sub> materials have

been theoretically predicted, for example, compounds IV, II-V and II-IV with zinc blend (ZB) structures, C-based materials with the elements Ca, Sr and Ba, rock structures (RS) and half-metallic ferromagnets (HM) in wurtzite (WZ) SrC. These compounds have interesting half-metallic behavior such as suitable spin-Flip gap and high Curie temperature [12].

The KCaX<sub>2</sub> (X= O, Ca, and N) were considered by Rozale et al., and reported a high half-metallic energy gap, high Curie temperature, and their resistance to lattice compression. Their work sought to study the half-metals known as d<sub>0</sub> in the half-Heusler structures, such as GeKC<sub>2</sub> and SnKC<sub>2</sub>. They retain half-metals, even if the lattice constant shrinks by about 10%, making it possible for materials to experience epitaxial growth on the surface of ordinary semiconductors without losing their HM properties.

In recent years, the discovery of two-dimensional (2D) systems has opened a new window toward nanotechnolo-

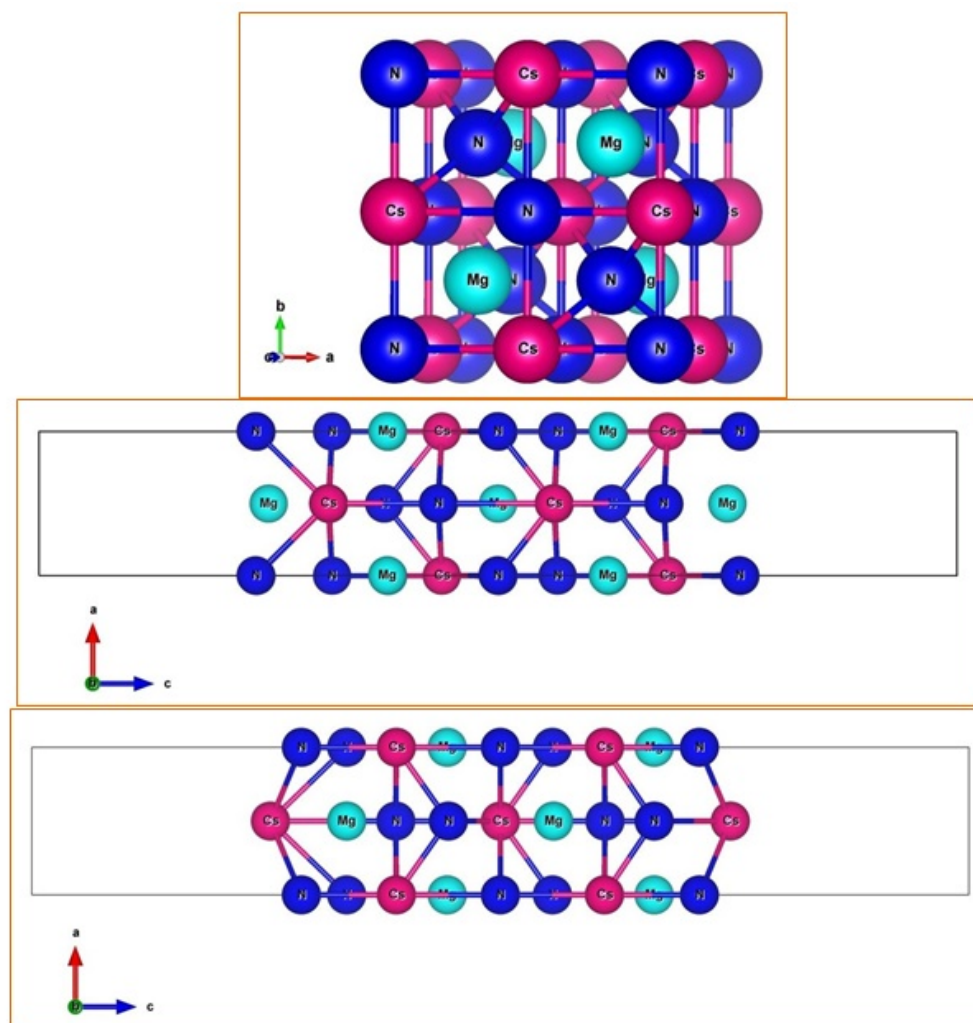


**Figure 1.** The structure of  $\text{CsMgN}_2$  and its films (Mg-N, and Cs-N terminations).

gies. The 2D compounds show new physical properties compared to their 3D compounds, such as copper oxides and certain iron compounds, based on their electrons correlation, at higher temperatures are the superconductor of its 2D form [13]. Some limitations in carbon graphene, such as the zero energy gap, it caused researchers to search for new two-dimensional structures. Therefore, many 2D structures such as  $\text{ZnS}$ ,  $\text{MoS}_2$ ,  $\text{MoTe}_2$ , etc. [14] have been researched. The half-Heusler (HH) alloys are the most fortunate for thermoelectric (TE) applications in power generation at room temperatures. The figure of merit (ZT) parameter is significant in showing the quality of thermoelectric properties if it is greater than one, and its value in n-type semiconductors is often greater than one [15]. Thermoelectric adaptability with industrial applications requires in-depth knowledge of their mechanical and electronic behavior [16–19]. This paper has calculated the structural properties of the  $\text{CsMgN}_2$  bulk, Cs-Mg, and Mg-N terminations. The electronic behaviors, including the density of states (DOS), band structures, electron density, and electrostatic potential diagrams, have been considered, and finally, the thermoelectric coefficients under temperature have been investigated.

## 2. Computational details

The mechanical, electronic, and optical results have been done by density functional theory (DFT) [20]. The Kohn-Sham equations [21] have been calculated by the full-potential linearized augmented plane wave (FP-LAPW) method [22] with Wien2K code [23]. The exchange-correlation potential, have approximated by the Perdew-Burke-Ernzerhof parameterization of the generalized gradient approximation (PBE-GGA) [24], and mBJ [25] for spin calculations. The optimized input parameters of RKmax, Gmax, Kpoint and lmax are selected to 8.0, 12,  $13 \times 13 \times 2$ , and 10, respectively. The muffin-tin radii (RMT) are set to 2.0 a.u. for all the atoms, and the separation energy is selected to be -8 Ry. The charge and energy convergence have been chosen to increase the accuracy of calculations to  $10^{-4}$  electrons and  $10^{-4}$  Ry. The calculations of the thermoelectric part have been done using BoltzTraP software [26]. In the calculations of thin film structures, due to the increase of atomic layers and the number of atoms, as well as the presence of vacuum on the surface of the films, the volume of calculations increases greatly. Therefore, we need to optimize the number of film layers. One of the suitable tools for

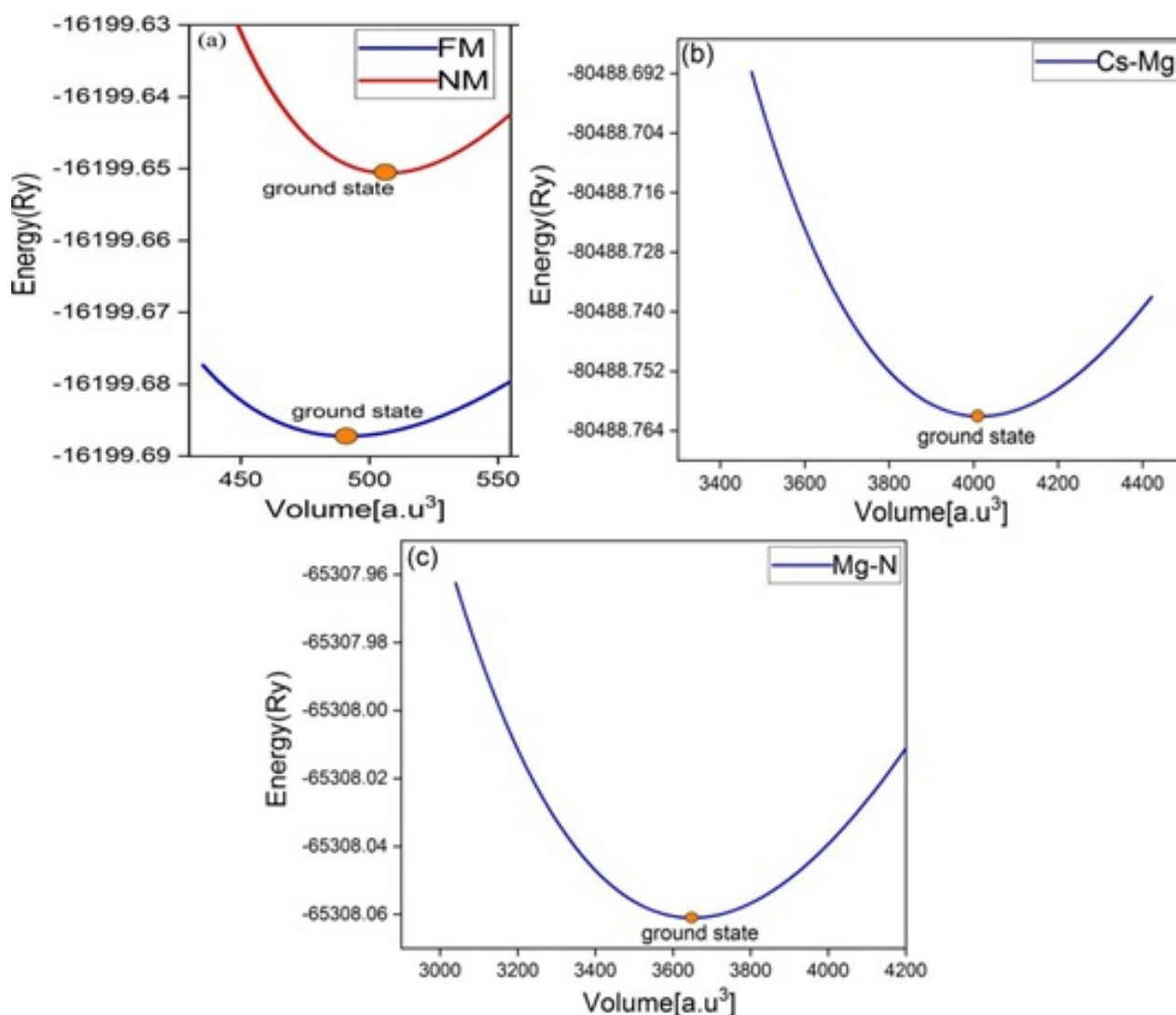


**Figure 2.** The E-V curve of (a) ferromagnetic and non-magnetic of CsMgN<sub>2</sub>, (b) Cs-Mg termination, and (c) Mg-N termination.

optimizing the number of layers is that the distance between the middle layers of the thin film, it should be equal to two consecutive layers in the bulk structure. Therefore, for our film structures, we first optimized their atomic forces to  $10^{-6}$  a.u./dyn, and then it was observed that for the mentioned layers, the distances between the middle layers is equal to the bulk structure. So the optimized layers of the Mg-N and Cs-Mg film terminations are 9 and 11 atomic layers, respectively.

### 3. Results and discussion

#### 3.1 Structural properties

Panel (a) of Figure (1) indicates the CsMgN<sub>2</sub> full-Heusler crystal structure. This compound has the FCC structure with atomic positions of Cs (0.5 0.5 0.5), Mg (0.75 0.75 0.75), N1 (0.0 0.0 0.0), N2 (0.25 0.25 0.25), and the F43m space group that has 24 symmetric matrices. Due to the various orbital shapes of the Cr [[Ar] 4s<sup>1</sup> 3d<sup>3</sup>], Mg [1s<sup>2</sup> 2s<sup>2</sup> 2p<sup>6</sup> 3s<sup>2</sup>], and N [1s<sup>2</sup> 2s<sup>2</sup> 2p<sup>3</sup>] atoms can promise new physical properties in this compound. In panels (b) and (c), the

Mg-N and Cs-Mg film terminations are depicted as having 9 and 11 atomic layers, respectively. In the middle layers, the film thickness of these cases must equal the bulk layers so the surface effects do not apply to the central layers. In these calculations, as mentioned in the computational method section, the forces acting on different atoms are optimized to  $10^{-6}$  a.u./dyn.

The free charges on the film surfaces caused create by dangling bonds cause an increase in the charge density. Also, the distance between the surface and subsurface layers changes, and an electrostatic force is applied to these layers. To indicate the mechanical stability from the static view, the total energy of the unit cells versus volume variation curves (E-V) of the bulk and Cs-Mg and Mg-N have been drawn in panels (a-c) of Figure (2). The E-V curves of the bulk phase are drawing in the ferromagnetic (FM), and non-magnetic (NM) phases and both diagrams have the ground state points with more stability in the FM phase than NM one. The E-V diagrams of the Cs-Mg and Mg-N terminations in panels (b) and (c) for the FM phase referred to their ground state points. It can be seen in the bulk phase that the curve arc in

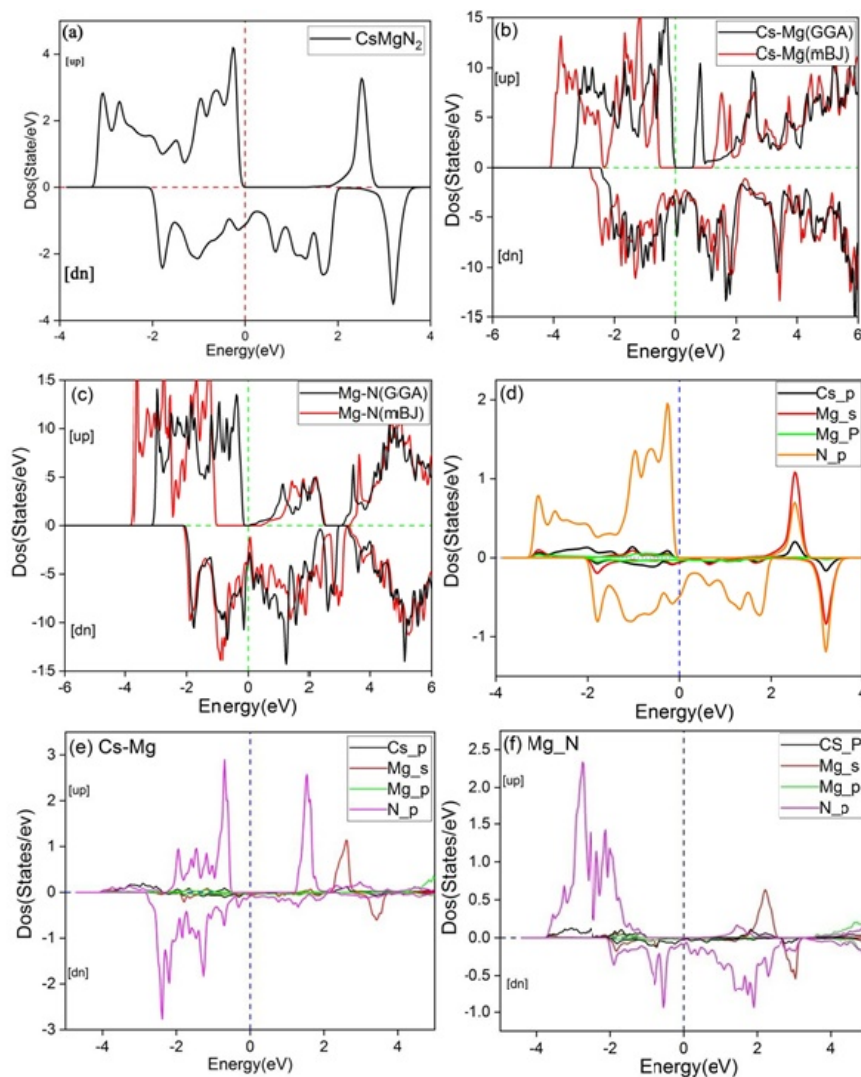


**Figure 3.** The DOS diagram of (a) the  $\text{CsMgN}_2$  bulk by GGA, (b) Cs-Mg termination by GGA and mBJ, (c) Mg-N termination by GGA, mBJ, and Partial DOS of (d) bulk with GGA, (e,f) Cs-Mg, and Mg-N terminations by mBJ.

the FM phase is less than the NM phase, indicating that the crystal stiffness in this phase will be less. All results from the E-V diagrams are summarized in Table 1 [12].

The bulk modulus of bulk and the Cs-Mg and Mg-N terminations are 35.2422 (GPa), 20.9015 (GPa), and 21.8669 (GPa), respectively. The bulk modulus derivatives in the bulk phase and the Cs-Mg termination indicate that the bonds tend to be ionic, and they tend to be covalent at the Mg-N termination. The magnetic moment in the bulk phase and the two terminations are integers conforming to the Slater–Pauling rule. The compound tends to be 100% spin polarization and exhibits half-metallic behavior. The presence of half-filled s and p orbitals in the orbitals of last layer of Cs and N atoms, in addition to the Heusler crystal structure of this compound, is the main reason for its ferromagnetic behavior in  $\text{CsMgN}_2$ . Also, the presence of Cs and N atoms on the surface of the Mg-N, and Cs-N terminations and the presence of surface free electrons of Cs:  $[\text{Xe}] 6s^1$ , and N:  $[\text{He}] 2s^2 2p^3$  on the surface of the films have increased the magnetic moment in the films. Also, the partial density of

states of p-orbital of N atom confirms it.

The reason for the difference in the magnetic moments of the Mg-N, and Cs-N terminations is that in the Mg-N termination, the Mg with the  $[\text{Ne}] 3s^2$ , orbital structure and N atoms with N:  $[\text{He}] 2s^2 2p^3$  orbital structure are in the surface, so, it is three free electrons in film surface, but at the Cs-N termination case, we have four free electron at the surface, then the magnetic moment of Cs-N termination is greater than other as we show at Table 1. One of the tools that shows that the structure of thin film films has been optimized is the distance between the layers. In Table 1, it can be seen that the distance between the middle layers is equal to the distance between two successive layers of the bulk, and are decreased below the film surfaces.

To show the stability of the Cs-Mg and Mg-N terminations structures from the energy point of view, we calculated the cohesive energy. Calculations showed that the value of cohesive energy for these structures was -6.45 (eV) and -6.89 (eV), respectively, which indicates their stability. Also, to emphasize the stability of these thin films, the enthalpy

**Table 1.** Lattice constants (a, c), distance layers of the crystals (d), equilibrium volume (V), Bulk modulus (B), and its derivative ( $\dot{B}$ ), ground state energy (E), total magnetic moment ( $M_{tot}$ ), and energy gap ( $E_{gap}$ ) of CsMgN<sub>2</sub> bulk, Cs-Mg and Mg-N terminations.(†: middle layer, and ‡: surface-subsurface layers)

Parameter	a (Å)	c (Å)	d (Å)	V [a.u. <sup>3</sup> ]	B (Gpa)	$\dot{B}$	E (eV)	$M_{tot}$	$E_{gap}$ (eV)
CsMgN <sub>2</sub> ,this work	6.62	...	1.65	491.0085	35.2422	5.2514	$-2.20 \times 10^5$	3.0	1.9 (GGA) 2.3 (mBJ)
CsMgN <sub>2</sub> [12]	6.50 [12]							3.0 [12]	2.4 [12]
film Cs-Mg[001]	4.76	30.21	1.65† 1.61‡	4014.0955	20.9015	5.2041	$-1.09 \times 10^6$	10	GGA=0.64 mBJ=1.81
film Mg-N[001]	4.61	29.27	1.64† 1.59‡	3649.7848	21.8669	3.3529	$-8.88 \times 10^5$	13.0	GGA=0.20 mBJ=1.60

was calculated. The results again emphasize the stability of these terminations and the Cs-Mg termination has more stability than other. The enthalpy is obtained for Cs-Mg termination 1.89 (eV), and Mg-N termination 1.12 (eV), respectively.

### 3.2 Electronic properties

The electronic properties of materials have always been of great help in studying optical, thermoelectric, and other physical properties. The electronic properties, including the density of states (DOS), the band structure, and the electron density (ED) diagrams of the CsMgN<sub>2</sub> compound and its films with the Cs-Mg and Mg-N terminations, have been examined. Figure (3), panels (a) to (f), displays the total and partial DOS diagrams of the CsMgN<sub>2</sub> compound and the Cs-Mg and Mg-N terminations in two spin channels up and down. From panel (a), it can be seen that the CsMgN<sub>2</sub> compound is a half-metal with full spin polarization at the Fermi level, as is expected from the magnetic moment of 3  $\mu$ B. The semiconductor form has a gap of 1.9 eV in the up spin and extreme metal in the down spin by GGA, and 2.3 (eV) with mBJ approximation which is agreed by Ref [12]. The electronic states are continuous and uniform and cut the Fermi level at a down spin. Therefore, it can be a magnetic switch for spintronic applications such as many Heusler films that are reported experimentally and theoretically [27–29].

The DOS diagrams of Cs-Mg and Mg-N terminations cases by GGA and mBJ approximations are depicted in panels (b) and (c). The Cs-Mg termination is half-metallic by 100% spin polarization at the Fermi level, and its energy gap increased by mBJ approximation to 2.1 eV of p-type semiconductor. In the up spin, the electronic states below the Fermi level mainly belong to the p orbitals of N atoms, which are the main factor to the electron injection above the Fermi level. As it can be seen in panel (d) for the CsMgN<sub>2</sub> bulk compound, the p orbitals of the N atom have the highest contribution in electronic states below the Fermi level in both spins. In the film with the Cs-Mg termination in the spin down, the continuity of electronic states can be detected from -2.5 (eV) to the positive energies, confirming the extreme metallic behavior. In panel (c), it can be seen that the Mg-N termination is converted to a half-metal with 100% spin polarization using both GGA and mBJ approxi-

mations. Applying the mBJ approximation, a wide gap can be seen in the up spin. This termination has become an n-type semiconductor, in which the electrons are the transport factor. Here, the main cause of the electronic states below and above the Fermi level belongs to the p orbital of the N atom. The energy gap in the bulk phase is in complete agreement with other reports, in the calculation of the band gap at the Cs-Mn and Mg-N terminations, due to the presence of free electrons on the surfaces of the films, in order to make the results more accurate, in addition to the GGA approximation, mBJ approximation was also used. The results showed that by applying the mBJ approximation, we see the splitting of electron states in high spin, the results of which are reported in Table 1.

### 3.3 Band structure

The CsMgN<sub>2</sub> bulk band structure and its two films of up and down spins are depicted in Figure (4). The n-type semiconductor with an indirect gap in up spin is witnessed, and the band dispersion is significant in the conduction region along the  $\Gamma$  direction, indicating high electron mobility. In the valance region, two significant gaps are also seen, but several levels are repeatedly cut off the Fermi level in the down spin of the bulk phase. In the Fermi and conduction regions, the levels slop are very high. In this spin, an energy gap of 6 eV is also observed at the valance region. The band structures of the Cs-Mg termination have been plotted in two up and down spins from panels (c) to (f) with GGA and mBJ approximations. It is quite clear that the mBJ approximation demonstrates n-type semiconductor properties with an indirect gap, and the condense levels are located below the Fermi level at up spin. The high density of states in the conduction zone guarantees their high conductivity. In panel (f), the Fermi levels are cut off by several levels many times, and this compound is a strong metal in this spin. Panels (g) to (j) illustrate the band structure of the Mg-N termination in two spins up and down. In both approximations, this termination is also a half-metal with 100% spin polarization, and the splitting of the states can be observed at the Fermi level by applying the mBJ approximation. However, it is a p-type semiconductor with an indirect gap in the up spin. Here, the high density of states in the valance region is also recognized as a good source of electron injection, but there is a 1.5 (eV) gap in the conduction region at this



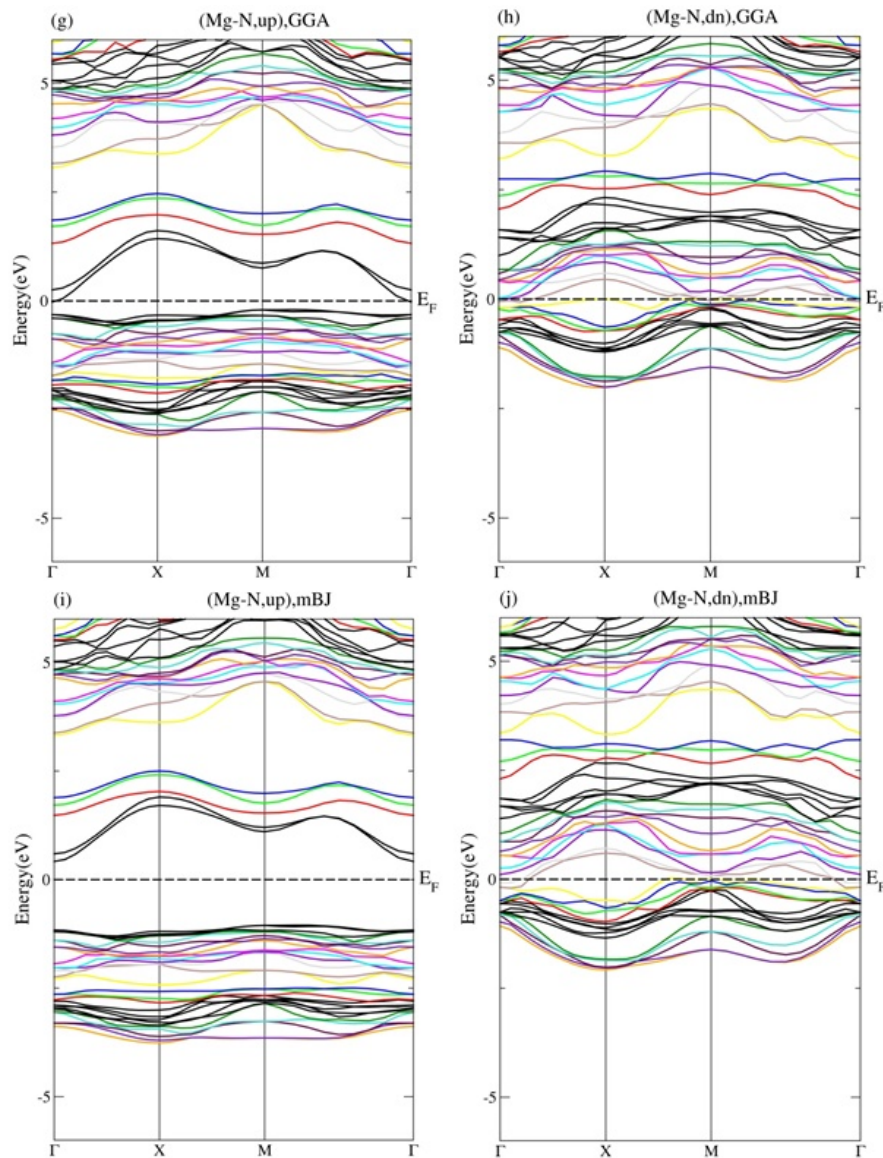


**Figure 4.** The bandstructure diagrams of CsMgN<sub>2</sub>, Cs-Mg, and Mg-N terminations.

termination. This reveals that electron leakage occurs here during the transport of the excited electrons. The excited electrons, which have reached the range of 0.5 to 2.2 (eV), are separated from the other states by another gap, which is suitable for the injected electron currents. This compound's extreme metal behavior in down spin demonstrates that this termination can be used as a proper tool in GMR and TMR applications.

Figure (5) displays the electron density on the surface of films with Cs-Mg and Mg-N terminations in two spins up and down. As can be seen from the grading of the figures by color, red has the highest electron density, and blue has the lowest one. In panels (a) and (b), by changing the spin from up to down, it is observed that the electron density, especially around the Cs atom, increases. Moreover, electron density changes are also more incredible at the film surface, but the shape of the electron density is more symmetrical in the middle layer. Thus, the effects of surface electrons on this compound's electronic and magnetic behavior are quite

obvious. Panels (c) and (d) have very interesting behavior; in the up spin, the orientation of the charge variation is inclined towards the Mg atom. Still, in the down spin, this orientation is shifted toward out of the film surface, indicating that the direction of the magnetic forces on the surface electrons varies as the direction of the external magnetic field changes. It also creates more significant multipolar polarity in the subsurface and middle layers' down spin. Interestingly, the electron density at the Mg-N termination confirms the strong magnetic character of this termination, which is reported in Table 1 to be  $13 \mu_B$ , so this termination is a very suitable option for spintronic purposes.

Due to the surface effects of Cs-Mg and also Mg-N terminations, as shown in Figures 5, the electron density on their surface have increased strongly in both up and down spins. An increase in the electron density on the film surfaces causes an increase in the electrostatic potential, as shown in Figure 6. Therefore, a large electrostatic force have been applied to the surface layer of the films and have

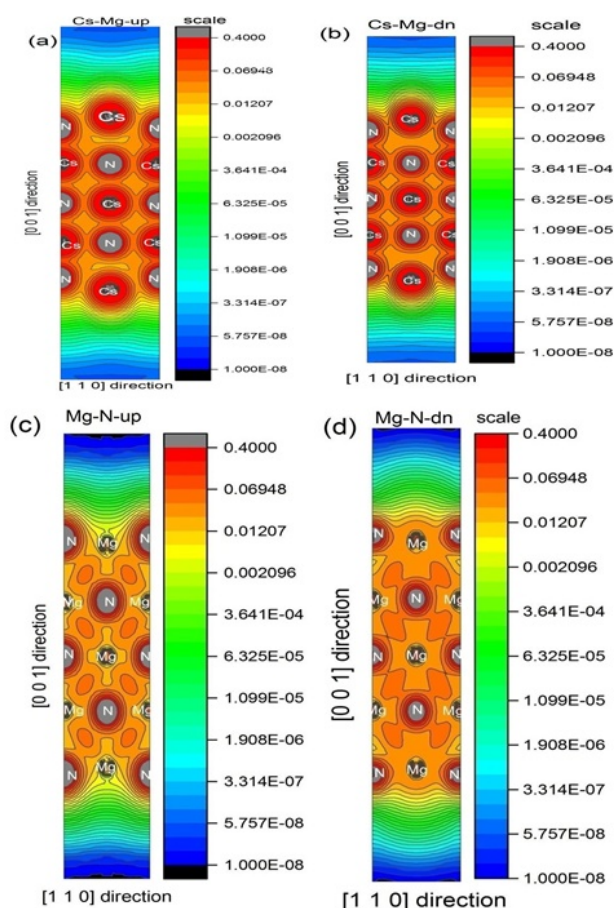


**Figure 5.** (a-d) The electron density diagrams of CsMgN<sub>2</sub>, Cs-Mg, and Mg-N terminations.

reduced the distance between the surface and the subsurface layers compared to the distance between the middle layers of the films. After forces optimizing atoms of the films, the distance between the middle layers at the Cs-Mg and also Mg-N terminations, was obtained to 1.61 (Å) and 1.64 (Å), and the distances of the surface with sub-surface layers of this terminations are 1.45 (Å), and 1.52 (Å), respectively.

Figure 6 displays the electrostatic potential at these two terminations. As can be seen from the figure, significant potential differences are detected between the surface and middle layers at the Cs-Mg and also Mg-N terminations, creating a large electrostatic force in the surface electrons. Still, this is much larger at the Mg-N termination, which is one of the reasons for the larger magnetic behavior at this termination. Additionally, this diagram illustrates that the electrons of the surface layers have large mobility due to the large force exerted on them at both terminations, especially the Mg-N one, which can be useful in the GMRs.

### 3.4 Thermoelectric properties

The thermoelectric property of the electric current is due to the temperature difference between two material points. Thermoelectric phenomena use to generate electronic current and measure temperature and cooling. One of the thermoelectric properties is the Seebeck effect, which was first discovered by the German scientist Thomas Johann

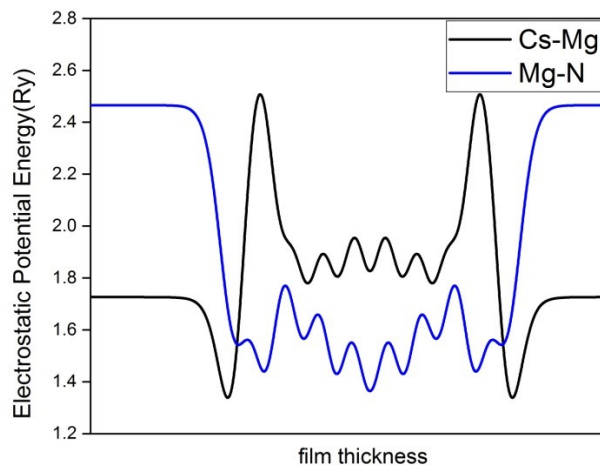


**Figure 6.** The electrostatic potential of Cs-Mg, and Mg-N terminations.

Seebeck in 1811. Seebeck concluded that the temperature difference in a circuit causes the charge carriers to move from hot points to cold ones, resulting in an electric field and potential difference. The Seebeck amount depends on factors such as the change of temperature and material type, and this coefficient also indicates the type of charge carriers. The negative sign of the Seebeck refers to the electron carriers of the n-type semiconductor, and the positive sign indicates the hole transporter of the p-type. The significant Seebeck coefficient refers to the big voltage by slight temperature difference. The figure of merit ( $ZT$ ) is a dimensionless coefficient that indicates the matter efficiency, and also power factor formula is collected below:

$$ZT = \frac{s^2 \sigma T}{K} \quad (1)$$

$$PF = S^2 \sigma \quad (2)$$

that  $T$  is the absolute temperature,  $S$  is the Seebeck coefficient,  $\sigma$  is the electrical conductivity and  $K$  is the thermal conductivity, including the lattice and electron contributions ( $K = K_{el} + K_{latt}$ ) [30–33].

Figure (7) plots the Seebeck coefficients, the electrical conductivity, and the thermal conductivity of the bulk and Cs-Mg and Mg-N thin films in their semiconductor phase (in spin down). Comparing the Seebeck coefficient of panels (a) and (b), it is observed that the Seebeck coefficient is positive in the bulk state and peaks at 150 K. Hence, the transport charge carriers are the holes, such as the Cs-Mg termination, which has a positive peak at 250 K. Nevertheless, the electrons are the transport charge carriers in the Mg-N termination, with a peak at 220 K. The magnitude of the Seebeck coefficient of the two thin films are greater than bulk case, and their peaks located at 200 K to 250 K temperature range, which referred to their better potential in thermoelectric than bulk structure. Since at down spin the CsMgN<sub>2</sub> compound and its films are semiconductors, so their electrical conductivity have the electrical gap. So that the electrical conductivity of the CsMgN<sub>2</sub> bulk starts from 300 K, and the electrical conductivity of Cs-Mg, and Mg-N terminations, starts from 480 K and 570 K, respectively.

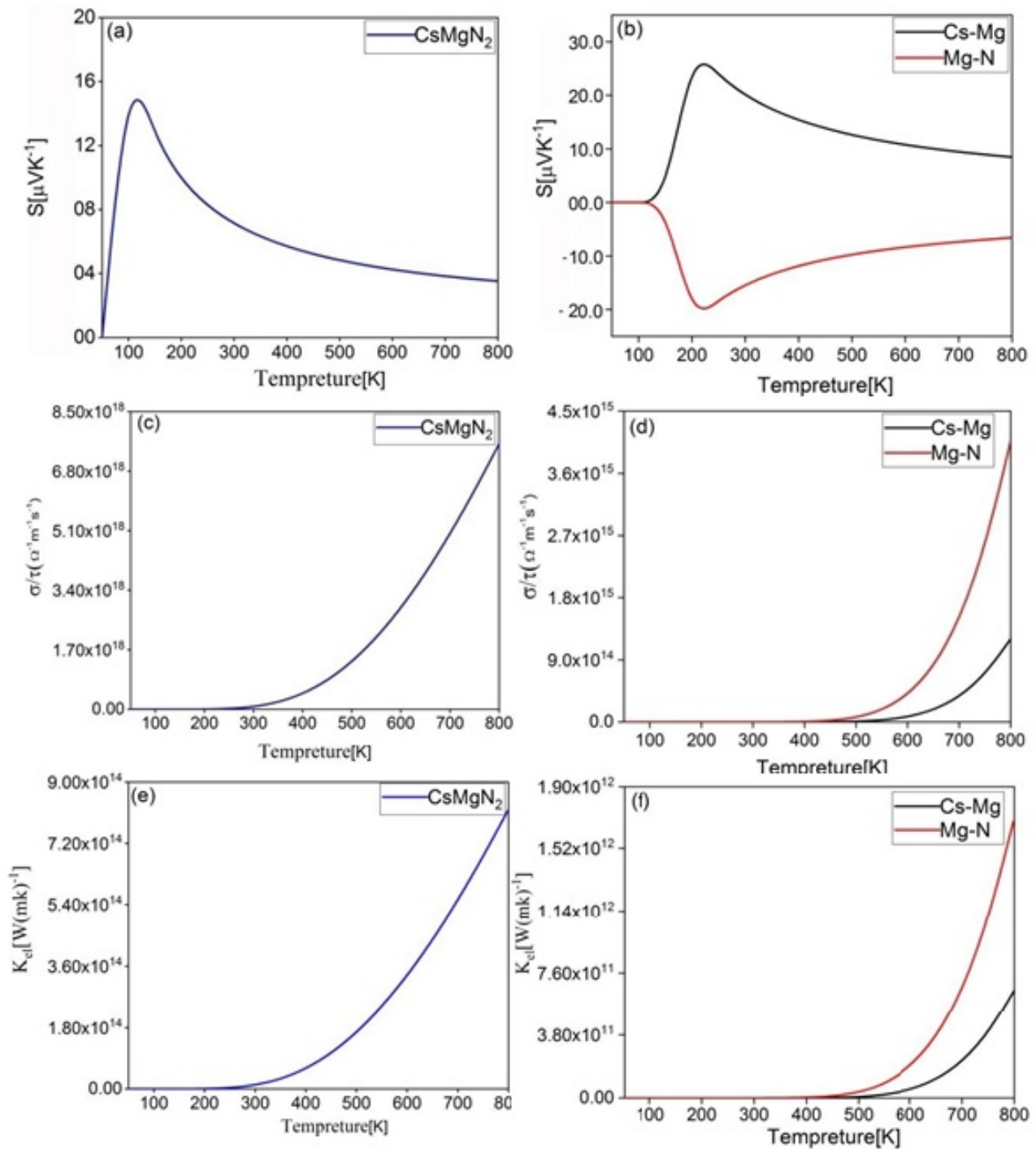


**Figure 7.** The Seebeck, electrical and thermal conductivity curves of the  $\text{CsMgN}_2$  bulk, and  $\text{Cs-Mg}$ , and  $\text{Mg-N}$  terminations versus temperature.

In panels (e) and (f), the thermal conductivity of the bulk and the films is again similar to the electrical conductivity, which its semiconductor nature is again confirmed here. Figure (8) shows the figure of merit (ZT) and power factor; in panels (a) and (b), the bulk ZT and the films are depicted in terms of temperature, indicating that both  $\text{CsMgN}_2$  and the mentioned films have a ZT. Accordingly, the ZT coefficient in the bulk phase is in the range of one and 0.9 in all temperature ranges. The  $\text{Cs-Mg}$  termination starts from one, while it begins from 0.95 in the  $\text{Mg-N}$  termination to

finally reach 0.85 at 800 K. These diagrams demonstrate that these compounds have high thermoelectric quality in thermoelectric applications. In panels (c) and (d), the power factor (PF) for these compounds shows that by increasing temperature, the PF coefficient increases with a steep slope, so they can be used in power generators. Many Heusler structure films also have thermoelectric behavior [34, 35]. It can be seen that the ZT coefficient is increasing at the  $\text{Cs-Mg}$  termination as room temperature and higher, while it is decreasing at the  $\text{Mg-N}$  termination and bulk case. There-

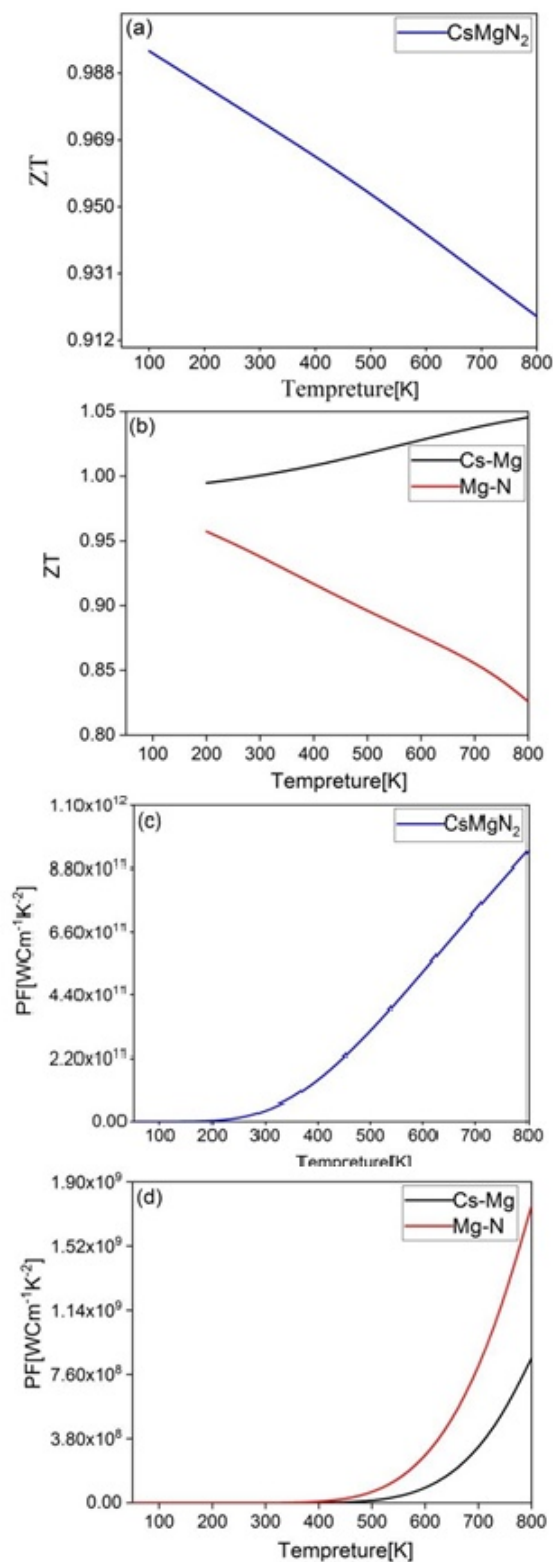


**Figure 8.** The figure of merit, and power factor of curves of the CsMgN<sub>2</sub> bulk, and Cs-Mg, and Mg-N terminations versus temperature.

fore, the Cs-Mg termination has a higher thermoelectric quality as well as the possibility of crystallization.

## 4. Conclusion

The electronic and thermoelectric properties of CsMgN<sub>2</sub> in bulk and its thin film at Cs-Mg and Mg-N terminations were investigated by DFT. It was observed that in the magnetic and non-magnetic states, the bulk and films have an equilibrium volume, and the two mentioned terminations have the ground state point. The total magnetic moment of all three compounds for the bulk and the Cs-Mg and Mg-N terminations are 3, 10, and 13 ( $\mu_B$ ), respectively. The derivative of the bulk modulus of these compounds represents strong ionic bonds in their atoms. The density of states curves and the band structure of bulk show that this compound is a strong half-metal with 100% spin polarization and a gap of 1.4 eV. The other two terminations experience half-metallic conditions with either the GGA approximation or mBJ one, but by applying the mBJ approximation, their spin-flip gap is larger in spin-up. It is observed that the Cs-Mg termination's Seebeck coefficient is positive at all temperatures, indicating the holes carriers to transport, as the bulk case, and in the Mg-N termination, the electrons are the charges transporter, because of its negative Seebeck parameter at all temperatures. The figure of merit coefficient of Cs-Mg and Mg-N terminations are like the bulk in the range of one. All three power factors are increasing at high temperatures, which refer to their power generator applications, especially the Mg-N termination case.

### Conflict of interest statement:

The authors declare that they have no conflict of interest.

## References

- [1] R. A. De Groot, F. M. Mueller, P. G. van Engen, and K. Buschow. "New class of materials: half-metallic ferromagnets". *Phys. Rev. Lett.*, **50**:2024, 1983.
- [2] K. Schwarz. "CrO<sub>2</sub> predicted as a half-metallic ferromagnet". *Journal of Physics F: Metal Physics*, **16**:L211, 1986.
- [3] I. Žutić, J. Fabian, and S. D. Sarma. "Spintronics: Fundamentals and applications". *Reviews of modern physics*, **76**:323, 2004.
- [4] J. de Boeck and G. Borghs. "Magnetoelectronics". *Phys. World*, **12**:27, 1999.
- [5] R. Kainuma, Y. Imano, W. Ito, Y. Sutou, H. Morito, S. Okamoto, O. Kitakami, K. Oikawa, A. Fujita, T. Kanomata, and K. Ishida. "Magnetic-field-induced shape recovery by reverse phase transformation". *Nature*, **439**:957, 2006.
- [6] T. Krenke, E. Duman, M. Acet, E. F. Wassermann, X. Moya, L. Ma nosa, A. Planes, E. Suard, and B. Ouladdiaf. "Magnetic superelasticity and inverse magnetocaloric effect in Ni-Mn-In". *Physical Review B*, **75**:104414, 2007.

- [7] T. Krenke, E. Duman, M. Acet, E. F. Wassermann, X. Moya, L. Manosa, and A. Planes. "Inverse magnetocaloric effect in ferromagnetic Ni–Mn–Sn alloys". *Nature materials*, **4**:450, 2005.
- [8] Z. D. Han, D. H. Wang, C. L. Zhang, S. L. Tang, B. X. Gu, and Y. W. Du. "Large magnetic entropy changes in the Ni<sub>45.4</sub>Mn<sub>41.5</sub>In<sub>13.1</sub> ferromagnetic shape memory alloy". *Appl. Phys. Lett.*, **89**:182507, 2006.
- [9] V. K. Sharma, M. K. Chattopadhyay, and S. B. Roy. "Large inverse magnetocaloric effect in Ni<sub>50</sub>Mn<sub>34</sub>In<sub>16</sub>". *J. Phys. D.*, **40**:1869, 2007.
- [10] S. Y. Yu, Z. H. Liu, G. D. Liu, J. L. Chen, Z. X. Cao, G. H. Wu, B. Zhang, and X. X. Zhang. "Large magnetoresistance in single-crystalline Ni<sub>50</sub>Mn<sub>50-x</sub>In<sub>x</sub> alloys ( $x = 14 - 16$ ) upon martensitic transformation". *Appl. Phys. Lett.*, **89**:162503, 2006.
- [11] V. K. Sharma, M. K. Chattopadhyay, K. H. B. Shaeb, A. Chouhan, and S. B. Roy. "Large magnetoresistance in Ni<sub>50</sub>Mn<sub>34</sub>In<sub>16</sub> alloy". *Appl. Phys. Lett.*, **89**:222509, 2006.
- [12] Y. C. Gao and X. T. Wang. "First-principle investigation of the  $d^0$  half-metallic properties in full-Heusler compounds CsAX<sub>2</sub> (A = Mg, Ca, Sr, and Ba; X = N, and O)". *Journal of the Korean Physical Society*, **66**:1160, 2015.
- [13] P. Farkačovský. "Superconducting correlations in the two-dimensional Hubbard model with long-range electron hopping". *Physica C: Superconductivity and its Applications*, **602**:1354141, 2022.
- [14] A. Boochani, M. Jamal, M. Shahrokhi, B. Nowrozi, M. B. Gholivand, J. Khodadadi, E. Sartipi, M. Amiri, M. Asshabi, and A. Yari. "Ti<sub>2</sub>VGe Heuslerene: theoretical prediction of a novel 2D material". *J. Mater. Chem.*, **7**:13559, 2019.
- [15] A. Yari, A. Boochani, and S. Rezaee. "Thermoelectric and optical properties of the SrS graphene by DFT". *Philosophical Magazine*, **100**:3108, 2020.
- [16] H. H. Xie, J. L. Mi, L. P. Hu, N. Lock, M. Chirstensen, C. G. Fu, B. B. Iversen, X. B. Zhao, and T. J. Zhu. "Interrelation between atomic switching disorder and thermoelectric properties of ZrNiSn half-Heusler compounds". *Cryst. Eng. Comm*, **14**:4467, 2012.
- [17] K. Kirievsky, Y. Gelbstein, and D. Fuks. "Phase separation and antisite defects in the thermoelectric TiNiSn half-Heusler alloys". *Journal of Solid State Chemistry*, **203**:247, 2013.
- [18] Y. Gelbstein, N. Tal, A. Yarmek, Y. Rosenberg, M. P. Dariel, S. Ouardi, B. Balke, C. Felser, and M. Köhne. "Thermoelectric properties of spark plasma sintered composites based on TiNiSn half-Heusler alloys". *J. Mater. Res.*, **26**:1919, 2011.
- [19] M. Gürth, G. Rogl, V. V. Romaka, A. Grytsiv, and E. Bauer and. "Thermoelectric high ZT half-Heusler alloys Ti<sub>1-x-y</sub>Zr<sub>x</sub>Hf<sub>y</sub>NiSn ( $0 \leq x \leq 1$ ;  $0 \leq y \leq 1$ )". *Acta Materialia*, **104**:210, 2016.
- [20] W. Kohn, A. D. Becke, and R. G. Parr. "Density functional theory of electronic structure". *Journal of Physical Chemistry*, **100**:12974, 1996.
- [21] W. Kohn and L. J. Sham. "Self-consistent equations including exchange and correlation effects". *Physical review*, **140**:A1133, 1965.
- [22] P. Blaha, K. Schwarz, P. Sorantin, and S. B. Trickey. "Full-potential, linearized augmented plane wave programs for crystalline systems". *Comput. Phys. Commun.*, **59**:399, 1990.
- [23] K. Schwarz, P. Blaha, and G. K. H. Madsen. "Electronic structure calculations of solids using the WIEN2k package for material sciences". *Computer physics communications*, **147**:71, 2002.
- [24] J. P. Perdew, K. Burke, and M. Ernzerhof. "Generalized gradient approximation made simple". *Physical review letters*, **77**:3865, 1996.
- [25] F. Tran and P. Blaha. "Accurate band gaps of semiconductors and insulators with a semilocal exchange-correlation potential". *Physical review letters*, **102**:226401, 2009.
- [26] G. K. H. Madsen and D. J. Singh. "BoltzTraP. A code for calculating band-structure dependent quantities". *Computer Physics Communications*, **175**:67, 2005.
- [27] A. Nabiałek, O. Chumak, A. Lynnyk, J. Z. Domagała, A. Pacewicz, B. Salski, J. Krupka, T. Yamamoto, T. Seki, K. Takanashi, L. T. Baczewski, and H. Szymczak. "Anisotropy of magnetoelastic properties in epitaxial Co<sub>2</sub>Fe<sub>x</sub>Mn<sub>1-x</sub>Si Heusler alloy thin films". *Physical Review B*, **106**:054406, 2022.
- [28] V. K. Kushwaha, S. Kokado, S. Kasai, Y. Miura, T. Nakatania, R. Kumara, H. Tajiri, T. Furubayashi, K. Hono, and Y. Sakuraba. "Prediction of half-metallic gap formation and Fermi level position in Co-based Heusler alloy epitaxial thin films through anisotropic magnetoresistance effect". *Phys. Rev. Materials*, **6**:064411, 2022.
- [29] E. H. Shourov, C. Zhang, P. M. Voyles, and J. K. Kawasaki. "Structure and magnetism in epitaxial Fe<sub>1+x</sub>Vsb nanocomposite films". *Physical Review Materials*, **5**:124605, 2021.
- [30] S. D. Guo and L. Qiu. "Thermoelectric properties of topological insulator BaSn<sub>2</sub>". *Journal of Physics D: Applied Physics*, **50**:015101, 2016.
- [31] D. K. Ko, Y. J. Keng, and C. B. Murray. "Enhanced Thermopower via Carrier Energy Filtering in Solution-Processable Pt-Sb<sub>2</sub>Te<sub>3</sub> Nanocomposites". *Nano letters*, **11**:2841, 2011.

- [32] L. MÜchler, F. Casper, B. Yan, S. Chadov, and C. Felser. “Topological insulators and thermoelectric materials”. *physica status solidi (RRL) – Rapid Research Letters*, **7**:91, 2013.
- [33] Y. V. Ivanov, A. T. Burkov, and D. A. Pshenay-Severin. “Thermoelectric Properties of Topological Insulators”. *Phys. Status Solidi B*, **255**:1800020, 2018.
- [34] H. Matsuura, M. Ogata, T. Mori, and E. Bauer. “Theory of huge thermoelectric effect based on a magnon drag mechanism: Application to thin-film Heusler alloy”. *Physical Review B*, **104**:214421, 2021.
- [35] J. Nag, D. Rani, D. Singh, R. Venkatesh, B. Sahni, A. K. Yadav, S. N. Jha, D. Bhattacharyya, P. D. Babu, K. G. Suresh, and Aftab Alam. “CoFeVSb: A promising candidate for spin valve and thermoelectric applications”. *Physical Review B*, **105**:144409, 2022.